The Astrophysical Journal Supplement Series, 174:504–513, 2008 February

LINE AND MEAN OPACITIES FOR ULTRACOOL DWARFS AND EXTRASOLAR PLANETS

Richard S. Freedman[1] and Mark S. Marley
NASA Ames Research Center, Mail Stop 245-3, Moffett Field, CA 94035-1000; freedman@darkstar.arc.nasa.gov

and

Katharina Lodders
Planetary Chemistry Laboratory, Department of Earth and Planetary Sciences, Washington University, Campus Box 1169, Saint Louis, MO 63130-4899; lodders@wustl.edu
Received 2007 March 27; accepted 2007 July 19

ABSTRACT

Opacities and chemical abundance data are crucial ingredients of ultracool dwarf and extrasolar giant planet atmosphere models. We report here on the detailed sources of molecular opacity data employed by our group for this application. We also present tables of Rosseland and Planck mean opacities, which are of use in some studies of the atmospheres, interiors, and evolution of planets and brown dwarfs. For the tables presented here we have included the opacities of important atomic and molecular species, including the alkali elements, pressure-induced absorption by hydrogen, and other significant opacity sources, but we neglect opacity from condensates. We report for each species how we have assembled molecular line data from a combination of public databases, laboratory data that is not yet in the public databases, and our own numerical calculations. We combine these opacities with abundances computed from a chemical equilibrium model using recently revised solar abundances to compute mean opacities. The chemical equilibrium calculation accounts for the settling of condensates in a gravitational field and is applicable to ultracool dwarf and extrasolar planetary atmospheres, but not circumstellar disks. We find that the inclusion of alkali atomic opacity substantially increases the mean opacities over those currently in the literature at densities relevant to the atmospheres and interiors of giant planets and brown dwarfs. We provide our opacity tables for public use and discuss their limitations.

Subject headings: line: profiles — molecular data — stars: atmospheres — stars: low-mass, brown dwarfs

Online material: machine-readable tables

1. INTRODUCTION

The thermal structure and radiative transfer within the atmospheres of ultracool dwarfs and extrasolar planets ultimately depends on an entire suite of molecular and atomic opacities relevant to the temperatures and pressures found in these objects. Our group utilizes these opacities in models of ultracool dwarfs and extrasolar planets (e.g., Marley et al. 2002; Fortney et al. 2006; Saumon et al. 2007) and provides them to other members of the community. Here we briefly summarize our current suite of molecular opacities that we depend on in our modeling and consider some relevant issues in their construction. We also report on the chemical equilibrium calculation used to compute molecular abundances.

Although less commonly used than in the past, some calculations, particularly of planetary evolution, utilize Rosseland (κ_R) or Planck (κ_P) mean opacities (e.g., Hubickyj et al. 2005). Canonically, Rosseland mean opacities are the appropriate choice for radiative transfer models of optically thick atmospheric regions where radiation propagates by diffusion, whereas Planck mean opacities are the appropriate choice in optically thin regions (Mihalas 1978). By their nature, mean opacities are sensitive to the sum of the relevant opacity sources involved in their computation. Changes both in molecular and atomic abundances and in the individual opacity sources themselves can impact the final product. Here we present improved calculations for both the abundance of atoms used in our equation of state and new calculations for the relevant opacity sources.

The best available data defining the "solar abundance" of the atoms has evolved over time as understanding of the Sun's atmospheric composition has improved. Here we employ solar and scaled solar metallicities that use the recently revised abundances presented in Lodders (2003). The chemical equilibrium gas compositions computed as a function of temperature and total pressure take condensate formation and condensate settling into clouds into account in the calculation of the chemical equilibrium as is appropriate for the conditions in brown dwarfs, extrasolar giant planets, and cool stars. However, we purposefully neglect grain opacity in the calculation of the Rosseland and Planck means. We emphasize that the results here do not apply to lower gravity environments such as protoplanetary disks because there the condensation chemistry, and therefore the gas chemistry, is significantly different than that in gravitationally bound atmospheres of substellar objects (Lodders 1999a; Lodders & Fegley 2002, 2006).

To compute mean opacities, we calculated a new set of molecular and atomic opacities on a grid of 324 pressure and temperature points ranging from 75 to 4000 K and 3×10^2 to 3×10^8 dyn cm^{-2} (3×10^{-4} to 300 bar). Every atomic and molecular line opacity in our database of 10 different gaseous species was included, and not simply a sampling. These opacities were computed on a fixed wavenumber grid that completely resolved individual line profiles. These opacities were then combined with collision-induced absorption due to interactions of hydrogen and helium as well as several other opacity sources. This new set of mean opacities uses the latest physical information including new terms due to alkali atoms that were not included in previous investigations. Condensate opacity is not included in the mean opacities presented here because condensate opacities depend on the particulars of cloud models chosen to model substellar atmospheres (e.g., Ackerman & Marley 2001) and may vary

[1] SETI Institute, Mountain View, CA.

greatly, depending on the actual thermal structure in a given situation. Because we neglect grain opacity, the opacities presented here should be regarded as a lower limit to the true opacity, which may be several orders of magnitude higher. The grain-free results are of interest as they highlight the important role of the alkali elements and isolate assumptions regarding the grain opacity.

Recent tabulations of mean opacities include the work by Lenzuni et al. (1991) for a zero metallicity gas and Ferguson et al. (2005). Tabulations from the latter work generally include opacity of solid condensates, but a few cases without grains are also presented. We compare our results to the latter work over the relatively limited region of overlap. No other pure gaseous opacity tables are readily available for solar metallicity over our temperature and pressure regime.

We discuss the opacity sources and methods for treating line broadening in § 2. In § 3 we discuss our chemical equilibrium calculation. Mean opacities are presented and discussed in § 4.

2. OPACITY SOURCES AND DATA

We maintain a large and constantly updated database of molecular and atomic opacities. Some of the opacities are from standard sources, such as the HITRAN database, while others are a mixture of standard and other sources. In this section we discuss the opacity sources we employ for each molecule of interest. Sharp & Burrows (2007) recently published a thorough discussion of molecular opacities for ultracool dwarfs and discuss which species are of greatest interest for modeling these objects. We refer the reader to that work for more extensive background discussions than are included here. Furthermore, several of the molecular and atomic opacity tabulations that they review are also employed by our group. Thus, for a number of opacity sources we simply defer to their discussion. In other cases, particularly for CH_4, our opacity line list is unique and we discuss it in some detail.

Given a list of atomic transitions, it is further necessary to compute a line shape for each atomic or molecular line. Thus, in § 2.2 we discuss our choices for molecular line shapes and pressure broadening.

2.1. *Molecular Opacities*

In this section we discuss the molecules for which we compute opacities (although many more species are included in the chemical equilibrium calculation). The selection of molecules is dictated by the chemistry in solar-composition brown dwarf and extrasolar giant planet atmospheres, and, to some extent, the availability of line data. Our list includes the most important opacity sources at the temperatures appropriate to our calculations as validated by observations of cool stars, brown dwarfs, and giant planets. We do not include certain sources that affect only the far-UV portion of the spectra as our high-temperature cutoff is currently 4000 K.

Most spectroscopic databases are built on measurements taken at or near room temperature, and theoretical calculations supply the missing transitions that can become important at high temperatures. If only room temperature databases are used, the transitions from highly excited energy levels (usually referred to as hot bands in the literature) would be missing and the true opacity at elevated temperatures would be substantially underestimated. Whenever possible, we use expanded databases here.

Note that all references to HITRAN are to the HITRAN database. The HITRAN Web site[2] provides the latest, updated data and copies of all the papers that give details on each molecule included.

[2] See http://cfa-www.harvard.edu/hitran.

H_2O.—The two most extensive line lists for water are those of Partridge & Schwenke (1997) and Barber et al. (2006). Both are computational lists with hundreds of millions of lines. We have made extensive comparisons between the two lists and find that over the temperature range relevant to brown dwarf and extrasolar planet atmospheres, the differences are slight. We utilize the former list here, supplemented with lines for minor isotopes ($HD^{18}O$ and $HD^{17}O$) from HITRAN.[3] The entire database includes about 2.9×10^8 lines. Line widths are computed using H_2 broadening data from Gamache (Gamache et al. 1998; R. R. Gamache 2001, private communication); a recent paper (Ma et al. 2007) discusses possible problems with the current implementation of this theory for some other molecules. However, the few examples shown in the Ma et al. paper only cover HF broadened by HF or N_2. The data for N_2-HF broadening showed little differences from the earlier theory, leading us to have some confidence in our approach until data is available for H_2 broadening of H_2O.

We note that Allard et al. (2000) and Jones et al. (2005) considered the completeness of the Schwenke H_2O (and TiO) databases at high temperature and concluded that the water database still lacked transitions from high vibrational energy levels needed for calculating models of M stars and proposed that a then preliminary (and never, to the best of our knowledge, publicly released) database by the Tennyson group was superior for these purposes. However, as discussed above, the latest release of the H_2O database from the Tennyson group Barber et al. (2006) no longer shows a significant difference with the earlier Schwenke result at these temperatures.

CH_4.—The laboratory analysis of the methane spectrum is incomplete and is unlikely to be completed from laboratory measurements alone. The difficulties arise from the high degree of symmetry of the molecule, which causes a great number of the bands to overlap, and the fact that the average line separation is generally less than the Doppler width at room temperature (Boudon et al. 2006).

The HITRAN methane database is not a true high-temperature database because many bands originating from higher vibrational levels are not included. Instead our line lists for $^{12}CH_4$ and $^{13}CH_4$ were generated using the latest Spherical Top Data System (STDS) software (Wenger & Champion 1998) from the group at the University of Bourgogne,[4] which allows us to calculate methane spectra to much higher total angular momentum value, J, than tabulated in HITRAN. For the calculations reported here we computed to a maximum rotational level of $J_{\max} = 60$, which likely covers lines of importance in cool objects. Homeier et al. (2003) also used the STDS software but only calculated up to $J_{\max} = 40$. For our calculation one band of $^{13}CH_4$ that is missing in the Bourgogne list was added from HITRAN and CH_3D was included from HITRAN. Extensive line width data for all bands is not available, so we separated the available information by reference to the vibrational symmetry of the transitions and applied it to all bands (L. Brown 1996, private communication). There are about 2×10^8 total CH_4 lines in the database. Figure 1 compares our computed hot methane opacity at 1000 K and 10^6 dyn cm^{-2} to an opacity computed solely from HITRAN data, both without any CH_3D. There is generally good agreement near band centers, and the computational database clearly provides important additions in regions where the HITRAN data are lacking. (See also Nassar & Bernath [2003] for lab data at high temperature.)

[3] In calculations specifically for brown dwarfs we set the deuterium abundance equal to zero; see § 3.1.

[4] See http://icb.u-bourgogne.fr/OMR/SMA/SHTDS/STDS.html.

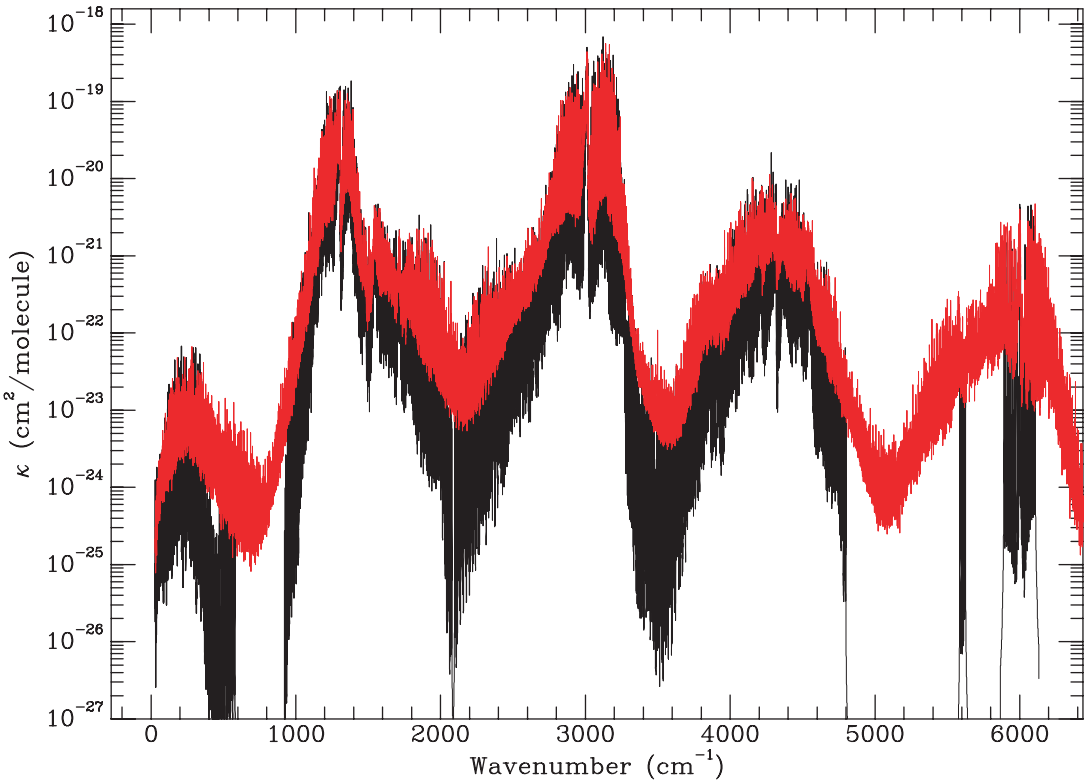

FIG. 1.—Opacity κ at 10^6 dyn cm^{-2} (1 bar) and 1000 K as a function of wavenumber for two opacity databases of the CH_4 molecule. Black data are computed from the standard HITRAN database. Red curve is derived from our computational database, as described in the text.

Both our database generated from the STDS software and HITRAN do not extend to wavenumbers much higher than about 6400 cm^{-1} (although many weak lines due to the $2\nu_3$ band extend up to 10,000 cm^{-1}). We thus supplement the numerical line database with a continuum opacity derived from laboratory data by Strong (Strong et al. 1993), even though the experimental results are not available at elevated temperatures. This situation is unlikely to improve until new theoretical predictions are available for CH_4. The currently available laboratory data for bands above 6400 cm^{-1} remained unanalyzed, in part because of lack of knowledge of the detailed energy levels of the transitions.

Recently, Leggett et al. (2007) compared our model spectra produced with the methane line list described above to the spectra of late-type T dwarfs. They found that the models still provide a poor match to observed spectra near 1.67 μm, where the models show too much flux. This is just the region where the calculated hot methane line list effectively ends except for the few very high J lines that extend to shorter wavelengths. We note that the CIA opacity of H_2-H_2 (see below) is predicted to vary rapidly with wavelength (by about a factor of 2) in this region. Thus, the inability to match the observations in this region could be ascribed either to the lack of good methane data, problems in the CIA simulations, or some combination of the two factors. It is also conceivable, but unlikely, that some other opacity source could also be missing from the models in this region. Further improvements to the methane opacity data will eventually resolve this problem.

NH_3.—For ammonia we rely on the line list from HITRAN supplemented with additional measurements, not yet fully analyzed, made at room temperature. These additional lines are in the 6600–7000 cm^{-1} region and are from the $\nu_3 + 2\nu_4$, $\nu_1 + \nu_3$, and the $2\nu_3$ bands (McBride & Nicholls 1972; L. Brown 2000, private communication). Only line strengths at 296 K and estimated values for the lower energy level are available for these bands. The final line list has about 34,000 lines. Line widths are computed as arising 90% from collisions with H_2 and 10% with He (from work by Nemchikov as reported in L. Brown 2000, private communication).

In their comparison of our spectral models for late T dwarfs to data, Leggett et al. (2007) also considered exploratory models that employed laboratory measurements of ammonia opacity by Irwin et al. (1999) over the spectral range of 0.91–1.9 μm. They found that even when atmospheric depletion of ammonia by nonequilibrium chemistry was accounted for, the predicted near-infrared ammonia features were not seen in the spectra of two T8 dwarfs. We conclude that the Irwin et al. data overestimate the ammonia opacity, and we do not employ that data set here.

CO.—As with methane, for carbon monoxide we favor a high-temperature line list over that available from HITRAN. We utilize the list from Goorvitch (1994), which includes bands that originate from highly excited energy levels. We supplement this list with data on $\Delta V = 4$ transitions from R. Tipping (1993, private communication) and somewhat fragmentary information on H_2 and He line widths from the literature (Bulanin et al. 1984; Le Moal & Severin 1986; Mannucci 1991). Minor isotopes missing from the Goorvitch list were added from HITRAN.

H_2S.—Data for the main isotope of H_2 ^{32}S are from a calculated list by R. Wattson (1996, private communication) plus minor isotopes from HITRAN. H_2 broadening was included from data in the literature (Kissel 2002). There are about 188,000 lines in the list. This list is not a true high-temperature list but does include many weak lines below the intensity cutoff of the current HITRAN line list. The wavenumber coverage is thus much greater than HITRAN, extending to 19,500 cm^{-1}.

PH_3.—For this molecule we use the latest HITRAN list, including new bands and broadening information from L. Brown (2000, private communication). The list includes about 20,000 lines.

TiO.—We include five isotopes in our TiO tabulation from Schwenke (1998) with modifications to the strengths of the δ and ϕ bands based on a comparison Allard et al. (2000) of models with stellar spectra. The list of about 1.7×10^8 lines includes transitions from higher energy levels. There is no data on broadening from H_2; instead we compare data from other species such as H_2S to try to set some reasonable limits on the broadening as discussed in § 2.2. The TiO molecular opacities should be reasonably complete for all temperatures considered, except perhaps for the very highest values considered in these tables (Allard et al. 2000).

As reported in Sharp & Burrows (2007), one of us (R. F.) discovered an error in line strengths in the program to convert the predictions of Schwenke (1998) from atomic units to HITRAN units, with the strengths being off by a multiplicative factor of $2J'' + 1$. This error is corrected here.

VO.—For this molecule we rely on the line list, consisting of about 3.1 million lines, from B. Plez (1998, private communication briefly reviewed in Sharp & Burrows 2007). No information on line broadening is available, so it is treated as was TiO.

FeH.—The line list for FeH is known to be incomplete in the near-infrared (Cushing et al. 2005). We rely on lists tabulated by Dulick et al. (2003) and discussed in more detail by Sharp & Burrows (2007). Only the most abundant ^{56}Fe isotope is used. No width data are available, so it was estimated by using data for similar molecules from the literature.

CrH.—For this molecule, primarily of interest in M and L dwarfs, we rely on a list from Burrows et al. (2002), which is further reviewed by Sharp & Burrows (2007). The list includes 55,300 lines, but again no width data are available and it was estimated.

2.2. *Line by Line Calculations*

As noted previously, we compute the opacity on a fine, fixed wavenumber grid. We add the opacity arising from each individual molecular line (hence, "line by line") using a program that takes information for each molecular absorber from a database that contains line strengths and positions, the lower energy level, and line-broadening information. The line profiles are generated from the line database with a Voigt profile algorithm; at higher pressures the profiles are essentially Lorentzian. We neglect the problem of how to treat the shape of the far line wings, where it is known (Levy et al. 1992) that the line shape should eventually become sub-Lorentzian. In most cases actual measurements, particularly at the higher pressures, are lacking and in many cases only a few theoretical predictions are available for selected bands. We make no attempt to simulate the specialized line shapes that are appropriate in the far IR and microwave regions (see de Pater et al. 2005 for a discussion in the context of Jupiter's deep atmosphere). The line shapes in these regions are expected to be asymmetric, but because of the large overlap of the low- and high-frequency wings due to the high density of lines, the effects due to the deviation of the line shape from a Lorentzian will tend to average out and should not cause a significant change in the integrated values of the mean opacities.

Likewise, we neglect χ factors (Levy et al. 1992) that describe the deviation of the line wings from a pure Lorenztian form. This includes effects such as line mixing and line narrowing, for example. Some information is available for selected species on the deviation of line shapes from a Lorentzian, but in many cases these studies have covered only a single band of a given molecular species, and the broadening agent was usually some mixture of N_2 and O_2 instead of H_2 and He, which would be the appropriate choice for brown dwarfs and giant planets. After conducting a number of tests, we found that the inclusion of a χ factor for H_2O, a major source of opacity, had no substantive effect on the Rosseland mean results. Considering all the other sources of uncertainty, we did not include χ factors in this study.

The collisional (pressure-broadened) line widths for several of the species used in our opacity calculations are not well known. In general, there have been no measurements reported in the literature and in many cases the main information about the line positions and intensities that we use comes from theoretical predictions. One could estimate, in principle, the line widths in comparison to other molecules by examining the relative values of the molecular polarizabilities (Hirschfelder et al. 1954; Lide 2000). Unfortunately, even this information is not available to us for many species of interest. It might be possible to again estimate some of these polarizabilities by quantum mechanical calculations, but again these data are not currently available. For the one case that can be compared to measurements, namely H_2S, the large relative value of the static polarizability compared to other molecules in our list does correlate well with the rather large line widths actually measured (Kissel et al. 2002). Currently, we simply use estimates for the line widths of TiO and the metal hydrides that are ~25%–50% larger than the line widths for other molecules that are earlier in the periodic table and generally have smaller effective radii when they are formed into molecules.

As a check on the effect of uncertainties in the line broadening for the various metal compounds, we calculated a set of TiO opacities with twice the assumed value of the pressure broadening widths. A direct comparison shows no significant effect on the overall mean opacity. The total value of the absorption is conserved over the line profile as it should be, assuming that the line wings are allowed to extend to larger values at higher pressures. The overall effect of broader lines is to smooth out the central peaks of the absorption lines and to fill in the low points in the far wings. Since the doubled widths approach the largest measured values for any molecule in our study (H_2S), it is apparent that line width uncertainties of a factor of 2 are not a significant source of error in our calculations.

The remaining line broadening parameters were taken from the literature when available. Available information can include actual measurements or theoretical predictions. In a few cases, no experimental or theoretical data of any kind for H_2 and He broadening were available, so estimates of the line width were made. In several cases, data were available for broadening by H_2 and He and this was used. The assumed line broadening parameters were scaled by pressure and an assumed temperature dependence for each (T, P) combination. This temperature dependence could come from actual measurements or from theory. In practice, the laboratory measurements do not cover a very large range in T, but this is usually all that is available (Homeier 2005). In contrast, the Van der Waals theory of broadening by foreign gases, commonly used in stellar atmospheres calculations, predicts the same temperature dependence for all lines irrespective of their angular momentum quantum numbers and the identity of the foreign broadener is usually assumed to be hydrogen atoms.

The scaling of the line width linearly with pressure ignores the problem of what happens to the line width at very high pressures, as a hard sphere cutoff to the pressure scaling should exist. This is related to the value of the second and higher virial coefficients in the equation of state for the gas. Since reliable experimental data on collision cross sections as derived from viscosity and diffusion data are only available for a few combinations of species and broadener, it is difficult to validate the theory under the physical conditions that apply to the astronomical case for more than a few molecule-broadener combinations. In particular, in the astronomical case the highest pressures are associated with

the highest temperatures, which is just the region where the parameters that determine the equation of state are the most uncertain.

2.3. *Collision-induced Absorption due to* H_2-H_2, H_2-He *and* H_2-H

Collision-induced absorption produces a broad continuum that sculpts the foundation of ultracool dwarf spectra. Our source for the subroutines to calculate the collision-induced absorption comes from the recent work of A. Borysow and her collaborators (Borysow 1991, 1992, 2002; Borysow et al. 1985, 1997, 2000; Birnbaum et al. 1996; Zheng & Borysow 1995; Borysow & Frommhold 1990). We have used the latest available versions of all programs to compute the CIA absorption due to H_2-H_2, H_2-He and H_2-H collisions. The Fortran programs and opacity tables available on Borysow's Web page[5] were used to construct tables that represent the absorption by a mixture of "normal" (3 : 1) H_2. This can be contrasted with an "equilibrium" mixture where the ratio of the ortho and para forms of H_2 is 1 : 1. At the high temperatures of these objects a normal distribution would be expected. This topic is discussed more thoroughly in Massie & Hunten (1982) and Carlson et al. (1992). In any case, the difference in the results between the two cases is only significant at the lowest temperatures and at the low-frequency end of the spectrum. This would lead to small changes in the results of a few percent in these cases, well within the other sources of uncertainty in this problem.

2.4. *Opacity from Alkali Atoms:* Na, K, Cs, Rb, *and* Li

The importance of alkali atoms to atmospheric opacity in cool substellar objects was first recognized from the influence of these atoms of the far red spectra of T dwarfs (Burrows et al. 2000). These pressure-broadened lines, particularly of Na and K, are major opacity sources over certain spectral ranges, temperatures, and densities, particularly above the Na and K condensation temperatures (about 600 K; Lodders 1999a). Although the exact form of the line shapes of the alkali atoms due to pressure broadening by H_2 is still not completely understood, it is important to include it. We use a computer code (Burrows et al. 2000) kindly provided to us by A. Burrows to generate line profiles for atomic lines of neutral alkali atoms using a line width parameter setting of 1.0 (as defined by those authors).

Burrows & Volobuyev (2003) and Allard et al. (2003) have further modeled the pressure-broadened alkali lines. Future improvements in understanding of the alkali line widths will certainly impact spectral modeling of ultracool dwarfs and may impact the mean opacities. The importance of the alkali elements to the mean opacities is discussed in § 4.

2.5. *Other Opacity Sources*

Several other opacity sources are included in our calculation. Bound-free absorption by H and H^- and free-free absorption by H, H_2, H_2^-, and H^- (see Lenzuni et al. 1991) were added using algorithms provided by T. Guillot (1999, private communication). Rayleigh scattering from H_2 and Thompson scattering are also included in the Rosseland mean following Lenzuni et al. Opacity from electrons and H atoms does not provide a large contribution to the overall opacity below ~2500 K but becomes important at higher temperatures relevant to M dwarf atmospheres.

The opacity from the more abundant atomic species are not important in our case because our high-temperature cases also involve high pressure. Since we are concerned with high-gravity objects the fractional abundances of atoms like Fe, Mg, Si, and Al never exceed 8×10^{-5} and are usually much lower. Furthermore, the most important lines for these atoms are in the UV where there is little flux over our temperature regime.

[5] See http://www.astro.ku.dk/~aborysow/.

3. CHEMICAL EQUILIBRIUM CALCULATIONS

The thermochemical equilibrium abundances used in the opacity models were computed with the CONDOR code described and applied to brown dwarf studies in several papers (e.g., Fegley & Lodders 1994, 1996; Lodders 1999a, 2002, Lodders & Fegley 2002). Brief overviews about the gas and cloud chemistry in substellar atmosphere can be found in Lodders (2004) and Lodders & Fegley (2006). Here we summarize this work and highlight important issues for the problem at hand.

3.1. *Gas and Condensate Chemistry Computations*

The CONDOR code simultaneously computes the chemical equilibrium compositions for more than 2200 gases (including ions) and more than 1700 solids and liquids of all naturally occurring elements by considering dual constraints of mass balance and chemical equilibrium. The major thermodynamic data sources are given in Fegley & Lodders (1994), and data are frequently updated (see, e.g., Lodders 1999b, 2004). Note that some frequently used compilations of thermodynamic properties and/or polynomial fits contain errors that also affect compounds important for brown dwarf chemistry (see Appendix 1 in Lodders 2002). Therefore, chemical equilibrium species and abundances computed by other groups could be different than our results if erroneous thermodynamic data were used by them, which can also introduce differences in calculated opacities.

The CONDOR code uses elemental abundances, total pressure and temperature as inputs. We use the solar system abundances in Lodders (2003), uniformly enhanced or depleted to model metallicity effects where appropriate. Equilibrium compositions considering cloud condensate formation for solar elemental abundances were computed for 324 pressure-temperature sample points in a grid ranging from 50 to 4000 K and $\log P(\mathrm{dyn\ cm^{-2}}) = 2$ to +8.5, which spans characteristic conditions in the atmospheres of low-mass objects. Similar calculations were done for other metallicities; here we only include results for metallicities of 2 and 1/2 times solar ($[\mathrm{M/H}] = \pm 0.3$).

Despite the plethora of gas species present in the thermochemical calculations, only a few compounds are abundant or major opacity sources, and the subset of the gases selected here for constructing the opacity tables are discussed in § 2. Compared to previous solar elemental abundance compilations, the more recent data include significant downward revisions in the C, N, and O abundances around 20%–40%, which have consequences for the abundances of important opacity sources such as methane, CO, water, and ammonia in substellar atmospheres. The new lower C, N, and O abundances resemble a decrease in CNO metallicity, and a detailed discussion of how metallicity affects the CH_4/CO and NH_3/N_2 equilibria is given in Lodders & Fegley (2002). For example, one important consequence of the lower C, N, and O abundances is that the methane to CO as well as the NH_3 to N_2 conversions are shifted toward higher temperatures (at constant total pressure or gravity) and are shifted toward lower total pressure (at constant temperature).

The thermochemical calculations also include results for deuterium. However, in the opacity modeling for brown dwarfs, the deuterium abundance was set to zero because it is assumed that all D is destroyed in objects more massive than 13 Jupiter masses. Thus, the opacities due from HDO and CH_3D are not included. However, in lower mass objects, the HDO and CH_3D opacities

must be included and these were calculated using $D/H = 1.94 \times 10^{-5}$ (Lodders 2003). However, the additional opacity from HDO and CH_3D generally has only a very marginal effect on the overall results.

3.2. *Condensate Treatment*

The CONDOR code has two principle pathways to treat condensate formation, depending on the desired application. Under ideal equilibrium conditions in protoplanetary disks or stellar winds, gas-solid equilibria are maintained within a cooling gas, and therefore high-temperature condensates that formed first from a cooling gas (primary condensates) still can react with the gas to form secondary condensates at lower temperatures. A well-known gas-solid reaction is the reaction of primary iron metal with H_2S gas to secondary troilite (FeS) at low temperatures (see below). However, such reactions may not apply to substellar atmospheres where cloud layer formation prevents the formation of secondary condensates (see Lodders & Fegley 2002). If a primary condensate settles from the gas into a cloud layer (sometimes called "rainout"), the primary condensate becomes depleted in the atmosphere above its cloud and cannot participate in reactions that are thermochemically favorable at the cooler temperatures above the cloud. For example, if iron metal condenses and settles into a cloud, the reaction of iron metal with H_2S to secondary troilite cannot happen. This has important consequences for the gas chemistry because troilite formation would remove all H_2S (essentially all the atmospheric sulfur inventory) at the low temperatures where troilite would be stable. However, if the secondary troilite does not form, H_2S remains in the atmosphere until NH_4SH condenses, which only happens at $T \ll 300$ K. The *Galileo* entry probe mass spectrometer detection of H_2S at about 3 times the solar S/H_2 ratio in Jupiter's atmosphere below the NH_4SH cloud level (Niemann et al. 1998) shows that the cloud layer condensation approach works well in giant planet atmospheres such as in Jupiter (see also Lodders & Fegley 2002; Visscher et al. 2006).

The computations with cloud settling thus require the knowledge of which condensates are primary (formed directly from the gas) and which ones are secondary (formed by gas-solid reactions). This is easily gauged from the equilibrium calculations by checking the distribution of an element between condensates and gas. For example, under typical total pressure conditions (e.g., $>10^5$ dyn cm^{-2}) in substellar atmospheres, iron starts to condense as metal at temperatures above 1600 K, and the metal settles into a cloud layer with a base at the temperature level where metal condensation starts. At the cloud base, iron metal is in evaporation-condensation equilibrium with the hotter atmosphere below. Above the cloud base, the iron gas abundance is determined by the iron vapor pressure of the metal cloud. The iron vapor pressure drops exponentially with the decreasing temperatures above the cloud, and mass balance dictates that more iron is in the condensates and less iron gas remains in the atmospheric gas. Typically, it takes about a 100–200 K drop from the condensation temperature (i.e., the temperature where the condensate appears first from a cooling gas) to the temperature where >99% of an element is removed by its condensate. This is the normal vapor-pressure–driven condensation process. The only special consideration here is that the condensate settles so that the amount of condensate becomes depleted at atmospheric levels above the condensate cloud that forms from the settled condensate particles. However, this does not affect the fact that the gas abundances remain established by the vapor pressure over the condensing solid or liquid because the vapor pressure over a substance is independent of the absolute amount of the substance present.

Troilite formation would only occur at temperatures below about 700 K, which is significantly lower than the temperatures at which iron vapor pressures are so low that essentially all iron is condensed. The gas-sold reaction for troilite formation requires the presence of iron metal, but at the temperature level where FeS becomes stable, the iron metal condensate has settled out at greater depth in low-mass object atmospheres, and thus, the secondary troilite cannot form.

Note that the thermochemical equilibrium calculations of the gas abundances do not require information about the cloud particle sizes, their settling efficiencies, or the vertical extent of the cloud layer; nor can these calculations provide this information without further model assumptions. These parameters are not needed if we are only interested in gas opacities, however, these parameters are needed if condensate opacities are to be considered, which requires inclusion of a detailed cloud model (see, e.g., Ackerman & Marley 2001; Marley et al. 2002).

Other observations also demonstrate that other refractory elements are depleted by condensate cloud formation at high temperatures deep in the atmospheres of low-mass objects. For example, the gradual disappearance of TiO and VO bands in the optical spectra of L dwarfs requires condensation of Ca-titanates into which VO dissolves (Fegley & Lodders 1994, 1996; Lodders 1999a, 2002). The absence of silane (SiH_4) indicates deeply seated silicate clouds and the presence of volatile germane (GeH_4) in the atmospheres of Jupiter and Saturn shows that germanium did not condense into iron metal at low temperatures (as it did in the solar nebula; see Lodders 2003) because the metal settled (Fegley & Lodders 1994). The presence of monatomic K gas in the atmospheres of T dwarfs requires that the refractory feldspar anorthite has settled into a deep cloud because otherwise, the more volatile K could dissolve in it at lower temperatures, (e.g., Lodders 1999a; Burrows et al. 2000; Geballe et al. 2001; Marley et al. 2002).

In summary, the major difference for *gas* chemistry between the "nebula" and "cloudy" cases is that the gas abundances of elements forming condensates by gas-solid reactions will be lower in the "nebula" models than in the "cloudy" models at the temperatures and total pressures where such secondary condensation is expected. In the cloudy models, the secondary condensates cannot form because the solid required for the gas-solid reaction is not present; e.g., anorthite is required for Na and K condensation in solid solution. Therefore, the *gas opacities* will be different for the nebula and cloudy models. As a practical matter, the biggest impact on the opacities arises from the timing of removal of gaseous alkali species. In the "cloudy" chemistry, Na and K persist to lower temperatures than would otherwise be the case. The spectra of T dwarfs confirms that in fact the "cloudy" chemistry is the correct choice for atmospheres. Since we neglect grain opacity, the differences in the timing and arrival of the condensates themselves does not impact our opacity calculation.

4. RESULTS

4.1. *Mean Opacity Tables*

Given the opacities described in § 2 and the elemental and molecular abundances described in § 3, we computed Rosseland and Planck mean opacities for three metallicities ($[M/H] = -0.3$, 0.0, $+0.3$). The integration over frequency was carried out using a grid of equally spaced wavenumber points. The frequency spacing was based on the temperature and pressure of each layer, such that the spectral resolution was always fine (1/4 of a line

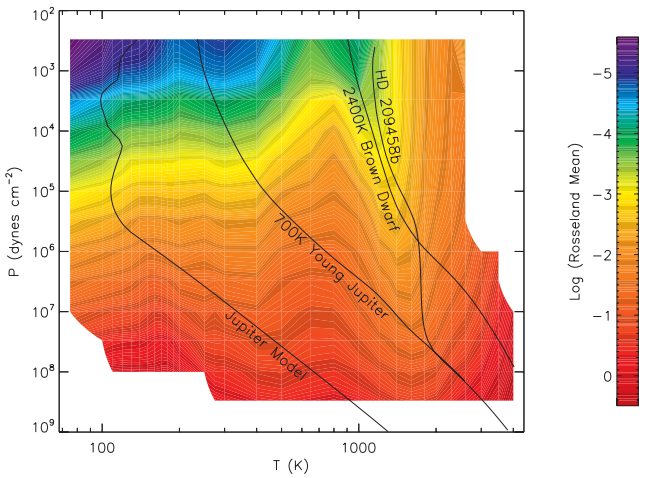

FIG. 2.—Contour plot showing Rosseland mean opacity over the temperature-pressure domain included in this study. Model temperature-pressure profiles from several planets and a brown dwarf are shown for comparison. Temperatures along profile refer to the effective temperature; brown dwarf profile is for an object with surface gravity $\log g(\mathrm{cm^2\ s^{-1}}) = 5$.

width or 0.5 $\mathrm{cm^{-1}}$, whichever is less) compared to a typical line profile under those conditions. Spacings are as small as 4×10^{-3} $\mathrm{cm^{-1}}$ in some instances. Such a fine grid is usually not required for mean opacity calculations, but we also use the same grid for high-resolution spectral modeling.

Our grid of 324 (P, T) pairs ranges from 75 to 4000 K and 3×10^2 to 3×10^8 dyn $\mathrm{cm^{-2}}$ (or 3×10^{-4} to 300 bar). We do not compute opacities at high pressure and low temperature or high temperature and low pressure, as such points are not reached by brown dwarf and giant planet atmosphere models. The table spacing is not uniform in order to better sample important processes, including water condensation. Figure 2 illustrates the pressure-temperature domain over which we computed opacities as well as the magnitude of the Rosseland mean opacities for a solar composition gas. This figure also shows temperature-pressure profiles computed for Jupiter and a variety of other substellar objects. Tables 1, 2, and 3 provide Rosseland and Planck mean opacities as a function of pressure and temperature for the three metallicities we consider on this grid. In the tables opacities have been converted to units of $\mathrm{cm^2\ g^{-1}}$ by calculating the mean molecular weight (for gaseous species only) at each temperature-pressure level, for each chemical composition.

Because of our choice of a uniform pressure-temperature (P, T) grid, our data are not on a uniform mass density (ρ) grid. For

TABLE 1

MEAN OPACITIES FOR [M/H] = 0.0

T (K)	P (dyn $\mathrm{cm^{-2}}$)	ρ (g $\mathrm{cm^{-3}}$)	κ_R ($\mathrm{cm^2\ g^{-1}}$)	κ_P ($\mathrm{cm^2\ g^{-1}}$)
75.....	3E+02	1.1277E−07	2.5619E−06	7.1083E−06
75.....	3E+03	1.1277E−06	2.5589E−05	6.4309E−05
75.....	1E+04	3.7591E−06	8.5261E−05	2.1238E−04
75.....	3E+04	1.1277E−05	2.5571E−04	6.3555E−04
75.....	1E+05	3.7591E−05	8.5211E−04	2.1167E−03
75.....	3E+05	1.1277E−04	2.5557E−03	6.3485E−03
75.....	1E+06	3.7591E−04	8.5180E−03	2.1160E−02
75.....	3E+06	1.1277E−03	2.5553E−02	6.3478E−02
75.....	1E+07	3.7591E−03	8.5176E−02	2.1159E−01
100.....	3E+02	8.4584E−08	4.5393E−06	2.4757E−02
100.....	3E+03	8.4583E−07	3.9962E−05	2.5407E−03
100.....	1E+04	2.8193E−06	1.2854E−04	1.0837E−03
100.....	3E+04	8.4582E−06	3.7709E−04	1.0589E−03
100.....	1E+05	2.8193E−05	1.2345E−03	2.5780E−03
100.....	3E+05	8.4582E−05	3.6583E−03	7.3903E−03
100.....	1E+06	2.8193E−04	1.2104E−02	2.4401E−02
100.....	3E+06	8.4582E−04	3.6260E−02	7.3044E−02
100.....	1E+07	2.8193E−03	1.2088E−01	2.4334E−01
100.....	3E+07	8.4582E−03	3.6261E−01	7.2982E−01

NOTE.—Table 1 is available in its entirety in the electronic edition of the *Astrophysical Journal Supplement*. A portion is shown here for guidance regarding its form and content.

TABLE 2

MEAN OPACITIES FOR [M/H] = +0.3

T (K)	P (dyn $\mathrm{cm^{-2}}$)	ρ (g $\mathrm{cm^{-3}}$)	κ_R ($\mathrm{cm^2\ g^{-1}}$)	κ_P ($\mathrm{cm^2\ g^{-1}}$)
75.....	3E+02	1.1313E−07	2.5527E−06	7.6946E−06
75.....	3E+03	1.1313E−06	2.5496E−05	6.4814E−05
75.....	1E+04	3.7710E−06	8.4951E−05	2.1216E−04
75.....	3E+04	1.1313E−05	2.5478E−04	6.3330E−04
75.....	1E+05	3.7710E−05	8.4894E−04	2.1074E−03
75.....	3E+05	1.1313E−04	2.5460E−03	6.3191E−03
75.....	1E+06	3.7710E−04	8.4845E−03	2.1060E−02
75.....	3E+06	1.1313E−03	2.5452E−02	6.3178E−02
75.....	1E+07	3.7710E−03	8.4837E−02	2.1059E−01
100.....	3E+02	8.4848E−08	4.5234E−06	2.4853E−02
100.....	3E+03	8.4846E−07	3.9824E−05	2.6108E−03
100.....	1E+04	2.8282E−06	1.2808E−04	1.1500E−03
100.....	3E+04	8.4846E−06	3.7575E−04	1.1219E−03
100.....	1E+05	2.8282E−05	1.2300E−03	2.6327E−03
100.....	3E+05	8.4846E−05	3.6443E−03	7.4225E−03
100.....	1E+06	2.8282E−04	1.2056E−02	2.4353E−02
100.....	3E+06	8.4846E−04	3.6115E−02	7.2772E−02
100.....	1E+07	2.8282E−03	1.2042E−01	2.4226E−01
100.....	3E+07	8.4846E−03	3.6123E−01	7.2650E−01

NOTE.—Table 2 is available in its entirety in the electronic edition of the *Astrophysical Journal Supplement*. A portion is shown here for guidance regarding its form and content.

TABLE 3

MEAN OPACITIES FOR [M/H] = −0.3

T (K)	P (dyn $\mathrm{cm^{-2}}$)	ρ (g $\mathrm{cm^{-3}}$)	κ_R ($\mathrm{cm^2\ g^{-1}}$)	κ_P ($\mathrm{cm^2\ g^{-1}}$)
75.....	3E+02	1.1260E−07	2.5662E−06	6.8130E−06
75.....	3E+03	1.1260E−06	2.5632E−05	6.4041E−05
75.....	1E+04	3.7535E−06	8.5404E−05	2.1245E−04
75.....	3E+04	1.1260E−05	2.5615E−04	6.3653E−04
75.....	1E+05	3.7535E−05	8.5363E−04	2.1208E−03
75.....	3E+05	1.1260E−04	2.5605E−03	6.3618E−03
75.....	1E+06	3.7535E−04	8.5345E−03	2.1205E−02
75.....	3E+06	1.1260E−03	2.5603E−02	6.3614E−02
75.....	1E+07	3.7535E−03	8.5343E−02	2.1205E−01
100.....	3E+02	8.4455E−08	4.5476E−06	2.4781E−02
100.....	3E+03	8.4453E−07	4.0027E−05	2.5126E−03
100.....	1E+04	2.8151E−06	1.2874E−04	1.0526E−03
100.....	3E+04	8.4453E−06	3.7770E−04	1.0280E−03
100.....	1E+05	2.8151E−05	1.2366E−03	2.5503E−03
100.....	3E+05	8.4453E−05	3.6650E−03	7.3736E−03
100.....	1E+06	2.8151E−04	1.2127E−02	2.4421E−02
100.....	3E+06	8.4453E−04	3.6329E−02	7.3175E−02
100.....	1E+07	2.8151E−03	1.2109E−01	2.4383E−01
100.....	3E+07	8.4453E−03	3.6325E−01	7.3143E−01

NOTE.—Table 3 is available in its entirety in the electronic edition of the *Astrophysical Journal Supplement*. A portion is shown here for guidance regarding its form and content.

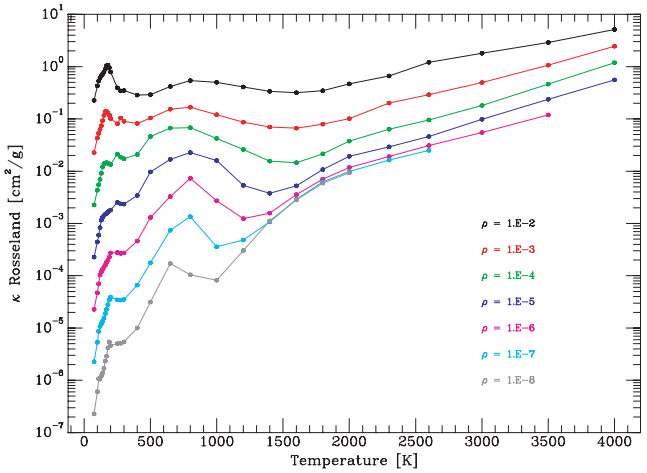

FIG. 3.—Rosseland mean opacity at seven densities as a function of temperature. Opacity data at each (ρ, T) pair is computed by interpolation within our standard grid. Some discontinuities in this figure arise from interpolation over chemical equilibria and condensation boundaries. Densities range from 1×10^{-8} (*bottom*) to 1×10^{-2} g cm^{-3}.

easier comparison with earlier work, we also interpolated to a set of constant densities for graphical purposes. Figure 3 illustrates the Rosseland mean opacities along profiles of constant density. We note that such an interpolation on occasions crosses chemical equilibria and condensation boundaries, which produces some kinks in the interpolated data shown on the figure.

4.2. *Opacity from Alkali Atoms:* Na, K, Cs, Rb, *and* Li

Perhaps the greatest difference from previous tabulations of mean opacities arises from the inclusion of the pressure-broadened lines of the alkali elements, particularly sodium and potassium. These molecules, with their large absorption cross sections in the far-red and very near-infrared (Burrows et al. 2000) fill what would otherwise be a region of fairly low opacity. Figure 4 compares the summed opacity as a function of wavenumber at 1400 K and 10^6 dyn cm^{-2} in our baseline case with a calculation that neglects the alkali opacity. The substantial role of the alkali opacity to the total summed opacity is unmistakable above about 10,000 cm^{-1}. The influence of the alkali opacity on the total gaseous mean opacity is illustrated in Figure 5, which compares the Rosseland mean opacity with and without the contribution of alkali metals at several densities. It is clear that at the higher densities the alkali opacity substantially fills in the opacity minimum from about 1000 to 1500 K. Differences at lower densities are slight since the pressure-broadened lines play a much smaller role.

Guillot et al. (1994a, 1994b) predicted that low opacity around 1000–2000 K in Jupiter's deep atmosphere would lead to the formation of a radiative region within what was then expected to be the fully convective deep interior of Jupiter. In Figure 2 it can be seen by extrapolation that Jupiter's deep adiabat indeed passes through a trough in opacity in this temperature range. We now understand that the opacity in this local minimum region—owing to the contribution of pressure-broadened alkali opacity—is much larger than was considered by Guillot et al. (1994a, 1994b) using the opacities available at that time. In a reevaluation of their earlier work, Guillot et al. (2004) indeed found that the alkali opacity is sufficient to prevent substantial energy transport by radiation in Jupiter's interior. The Rosseland opacities we report here are consistent with those used in the latest work by Guillot and collaborators. Thus, despite the intrinsic uncertainty in the alkali line widths at high pressure, a thin radiative shell within the interior of Jupiter need not be considered in the construction of interior

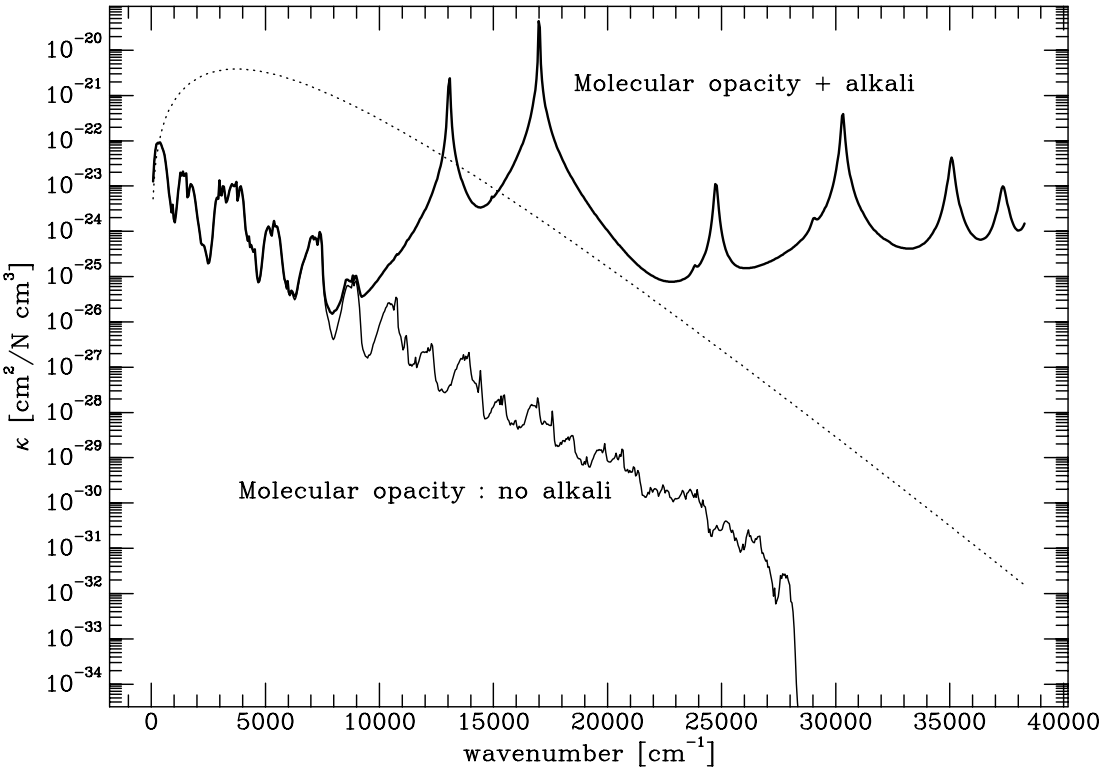

FIG. 4.—Total opacity as a function of wavenumber at 1400 K and 1 bar. Thin curve gives opacity without the contribution of alkali atoms. Thicker curve shows summed opacity including alkalis, computed using the theory of A. Burrows (1999, private communication). Under these conditions the alkali opacity dominates at wavenumbers above about 10,000 cm^{-1}. The derivative of the Planck function, dB/dT, which weights the opacity in the computation of the Rosseland mean, is shown as a dotted line on an arbitrary log scale.

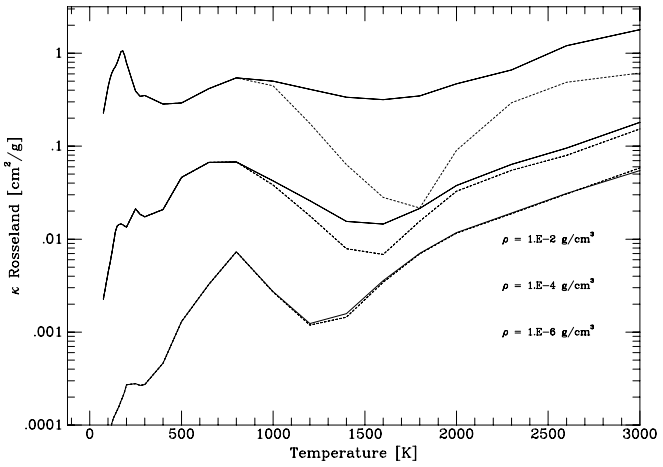

FIG. 5.—Rosseland mean opacity at three densities as a function of temperature. Opacity data at each (ρ, T) pair is computed by interpolation within our standard grid. Some discontinuities in this figure arise from interpolation noise. Densities range from 1×10^{-6} (*bottom*) to 1×10^{-2} g cm^{-3}. Solid line denotes our standard calculation, and the dotted line represents a case with the alkali opacity set equal to zero. The alkali opacity substantially increases the mean opacity at high densities and temperatures above about 1000 K. Differences in the lowest density case plotted are negligible.

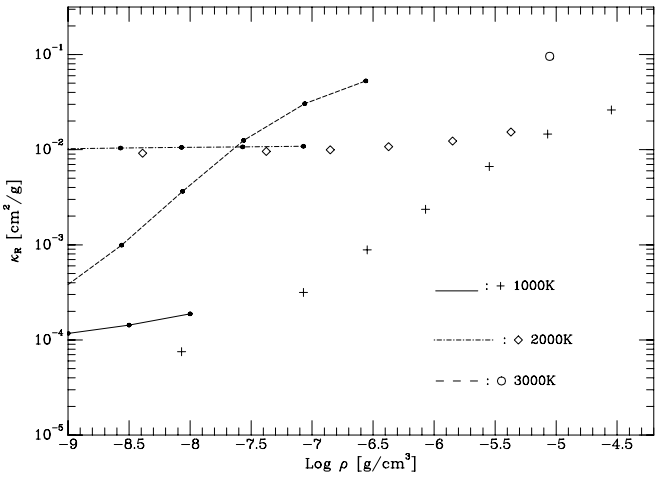

FIG. 6.—Rosseland mean opacity as a function of density for three temperatures. Solid and dashed lines are the "no-grain" opacity from Ferguson et al. (2005) for three temperatures (specifically their case with $X = 0.7$ and $Z = 0.02$, filename "cunha06.nog.7.02.tron"). This opacity database is optimized for protostellar disks and thus there is relatively little overlap in density space with the cool atmospheric conditions we consider here. The closest densities from our calculation (including alkali opacity) are shown as isolated symbols. There is excellent agreement at 2000 K. The trends for 1000 and 3000 K suggest reasonably good agreement between the two calculations.

models. This removes one source of uncertainty in the construction of evolution and interior models of Jupiter.

As noted in § 2.4, the pressure-broadened line shape for the alkali metals remains uncertain, particularly at high pressure. In the future, it may be possible to obtain experimental data on the line absorption coefficients of pressure-broadened alkali lines so that the effects of their shapes on the total opacity can be quantified to replace the semiempirical profiles (Johnas et al. 2006).

5. DISCUSSION

The opacities and chemical equilibrium calculations described here are examples of the current state of the art for understanding giant planet and brown dwarf atmospheres. Nevertheless, a number of uncertainties remain, particularly in the treatment of the opacities at high temperatures. Because it is a dominant source of opacity, of course water is of special concern, but comparisons between the most recent theoretical line lists suggest that, at least for the temperatures considered here, the line list is in reasonably good shape. Further work on calculating an updated version of the water spectrum is currently underway. Missing opacity at high temperatures is certainly a problem in even greater measure for most of the other molecular opacities, particularly methane, but these other molecules are generally less important than water to the mean opacity. In fact, only water, CO, TiO, and to a lesser extent VO have a significant contribution from hot bands, while CH_4 and, to a lesser extent, H_2S contain lines originating from higher rotational quantum values that have been predicted from a mixture of theory and available experimental data.

For comparisons with spectra of ultracool dwarfs, however, the lack of adequate high-temperature opacities for methane and ammonia is an important limitation (e.g., Leggett et al. 2007). Improving this situation will require in the case of methane a substantial theoretical and computational effort. Newer data are under development for water by D. Schwenke and for CO by one of us (R. F.) that would allow a recomputation of the line lists. In the case of water, this could lead to a better representation of the opacity at the highest temperatures, while any changes in the CO database will probably be less substantial.

Because the calculations presented here do not include condensates as an opacity source a direct comparison with earlier work that includes grains is difficult. In our brown dwarf and extrasolar planet modeling calculations cloud opacity is computed from the local description of the atmospheric structure, rather than relying on a precomputed table. Because these additional sources of opacity may appear at different pressures and temperatures in a series of models depending on the assumptions built into the calculation, it is not possible to give a general set of results that include solid material. Any such tables must be regarded with some caution as condensate size and abundance depends on other parameters, including the convective velocity, and no single prescription as a function of only density and temperature can be given. In fact the grain opacity plays an important role in the gaseous accretion of giant planets by the core accretion mechanism (Hubickyj et al. 2005).

We show in Figure 6 a comparison with recent grain-free calculations (Ferguson et al. 2005). This work uses updated atomic abundances to compute mean opacities at relatively low densities relevant to circumstellar disks. As such the region of overlap in density and temperature is relatively small. In the overlapping region, however, the correspondence is reasonably good. Since this is a low-density region, the effect of the alkali opacity is negligible and is not a factor.

6. CONCLUSION

The tables presented here and in the on line supplement to this paper provide Rosseland and Planck mean opacities for three elemental compositions relevant to the study of ultracool dwarfs and extrasolar giant planets. We have also described the databases for line transitions and our approach to computing the line broadening as well as the chemical equilibrium calculation. Future improvements in the molecular opacities—particularly at high temperature—will certainly improve the quality of model spectra for the comparison with astronomical data. Barring the addition of substantial new opacity sources or further updates to the solar abundance of the elements, we do not expect to see significant changes to the Rosseland and Planck mean opacities reported here.

We thank Tristan Guillot for providing his hydrogen opacity routine and for helpful advice, Jonathan Fortney for help with figures and formatting, Didier Saumon for helpful conversations, Adam Burrows for use of his alkali atom opacity code, and the referee for suggestions that improved the manuscript. We also received generous support from David Schwenke and his collaborators. He has provided extensive calculations and information concerning the quantum mechanical modeling of various spectra. R. F. acknowledges support from NASA grant NAG5-4970, M. M. acknowledges support from the NASA Office of Space Sciences. Work by K. L. is supported by NSF grant AST 04-06963 and NASA grant NNG06GC26G.

REFERENCES

Ackerman, A. S., & Marley, M. S. 2001, ApJ, 556, 872
Allard, F., Hauschildt, P. H., & Schwenke, D. 2000, ApJ, 540, 1005
Allard, N. F., Allard, F., Hauschildt, P. H., Kielkopf, J. F., & Machin, L. 2003, A&A, 411, L473
Barber, R. J., Tennyson, J., Harris, G. J., & Tolchenov, R. N. 2006, MNRAS, 368, 1087
Birnbaum, G., Borysow, A., & Orton, G. S. 1996, Icarus, 123, 4
Borysow, A. 1991, Icarus, 92, 273
———. 1992, Icarus, 96, 169
———. 2002, A&A, 390, 779
Borysow, A., Borysow, J., & Fu, Y. 2000, Icarus, 145, 601
Borysow, A., & Frommhold, L. 1990, ApJ, 348, L41
Borysow, A., Jorgensen, U. G., & Zheng, C. 1997, A&A, 324, 185
Borysow, J., Trafton, L., Frommhold, L., & Birnbaum, G. 1985, ApJ, 296, 644
Boudon, V., Rey, M., & Lõete, M. 2006, J. Quant. Spectrosc. Radiat. Transfer, 98, 394
Bulanin, M. O., Dokuchaev, A. B., Tonkov, M. V., & Filippov, N. N. 1984, J. Quant. Spectrosc. Radiat. Transfer, 31, 521
Burrows, A., Marley, M., & Sharp, C. 2000, ApJ, 531, 438
Burrows, A., Ram, R. S., Bernath, P., Sharp, C. M., & Milsom, J. A. 2002, ApJ, 577, 986
Burrows, A., & Volobuyev, M. 2003, ApJ, 583, 985
Carlson, Barbara, E., Lacis, Andrew, A., Rossow, & William, B. 1992, ApJ, 393, 357
Cushing, M. C., Rayner, J. T., & Vacca, W. D. 2005, ApJ, 623, 1115
de Pater, I., Deboer, D., Marley, M., Freedman, R., & Young, R. 2005, Icarus, 173, 425
Dulick, M., Bauschlicher, C. W., Jr., Burrows, A., Sharp, C. M., Ram, R. S., & Bernath, P. 2003, ApJ, 594, 651
Fegley, B., Jr., & Lodders, K. 1994, Icarus, 110, 117
———. 1996, ApJ, 472, L37
Ferguson, J. W., Alexander, D. R., Allard, F., Barman, R., Bodnarik, J. G., Hauschildt, P. H., Heffner-Wong, A., & Tamanai, A. 2005, ApJ, 623, 585
Fortney, J. J., Saumon, D., Marley, M. S., Lodders, K., & Freedman, R. S. 2006, ApJ, 642, 495
Gamache, R. R., Lynch, R., & Neshbya, S. P. 1998, J. Quant. Spectrosc. Radiat. Transfer, 59, 319
Geballe, T. R., Saumon, D., Leggett, S. K., Knapp, G. R., Marley, M. S., & Lodders, K. 2001, ApJ, 556, 373
Goorvitch, D. 1994, ApJS, 95, 535
Guillot, T., Chabrier, G., Morel, P., & Gautier, D. 1994a, Icarus, 112, 354
Guillot, T., Gautier, D., Chabrier, G., & Mosser, B. 1994b, Icarus, 112, 337
Guillot, T., Stevenson, D. J., Hubbard, W. B., & Saumon, D. 2004, in Jupiter: The Planet, Satellites and Magnetosphere, ed. F. Bagenal, T. E. Dowling, & W. B. McKinnon (Cambridge: Cambridge Univ. Press), 35
Hirschfelder, J. O., Curtiss, C. F., & Bird, R. B. 1954, Molecular Theory of Gases and Liquids (New York: Wiley)
Homeier, D. 2005, Mem. Soc. Astron. Italiana, 7, 157
Homeier, D., Hauschildt, P. H., &, Allard, F. 2003, ASP Conf. Ser. 288, Stellar Atmosphere Modeling, ed. I. Hubeny, D. Mihalas, & K. Werner (San Francisco: ASP), 357
Hubickyj, O., Bodenheimer, P., & Lissauer, J. J. 2005, Icarus, 179, 415
Irwin, P. G. J., Calcutt, S., B., Sihra, K., Taylor, F. W., Weir, A. L., Ballard, J., & Johnston, W. B. 1999, J. Quant. Spectrosc. Radiat. Transfer, 62, 193
Johnas, C. M. S., Allard, N. F., Homeier, D., Allard, F., & Hauschildt, P. H. 2006, in AIP Conf. Proc. 874, Spectral Line Shapes XVIII (New York: AIP), 354
Jones, H. R. A., Pavlenko, Y., Viti, S., Barber, R. J., Yakovina, L. A., Pinfield, D., & Tennyson, J. 2005, MNRAS, 358, 105
Kissel, A., Sumpf, B., Kronfeldt, H.-D., Tikhomirov, B. A., & Ponomarev, Yu. N. 2002, J. Mol. Spectrosc., 216, 345
Leggett, S., Marley, M. S., Freedman, R., Saumon, D., Liu, M. C., Geballe, T. R., Golimowski, D., & Stephens, D. 2007, ApJ, 667, 537
Le Moal, M. F., & Severin, F. 1986, J. Quant. Spectrosc. Radiat. Transfer, 35, 145
Lenzuni, P., Chernoff, D. F., & Salpeter, E. E. 1991, ApJS, 76, 759
Levy, A., Lacome, N., & Chackerian, C., Jr. 1992, Spectroscopy of the Earth's Atmosphere and Interstellar Medium (Burlington: Academic Press)
Lide, D. R., ed. 2000, Handbook of Chemistry and Physics (81st ed.; Boca Raton: CRC Press)
Lodders, K. 1999a, ApJ, 519, 793
———. 1999b, J. Chem. Phys. Ref. Data, 28, 1705
———. 2002, ApJ, 577, 974
———. 2003, ApJ, 591, 1220
———. 2004, Science, 303, 323
———. 2002, Icarus, 155, 393
———. 2006, in Astrophysics Update 2, ed. J. W. Mason (Berlin: Springer), 1
Ma, Q., Tipping, R. H., & Boulet, C. 2007, J. Quant. Spectrosc. Radiat. Transfer, 103, 588
Mannucci, A. J. 1991, J. Chem. Phys., 95, 7795
Marley, M. S., Seager, S., Saumon, D., Lodders, K., Ackerman, A. S., Freedman, R. S., & Fan, X. 2002, ApJ, 568, 335
Massie, S. T., & Hunten, D. M. 1982, Icarus, 49, 213
McBride, J. O. P., & Nicholls, R. W. 1972, J. Phys. B, 5, 408
Mihalas, D. 1978, Stellar Atmospheres (2nd ed; San Francisco: Freeman)
Nassar, R., & Bernath, P. 2003, J. Quant. Spectrosc. Radiat. Transfer, 82, 279
Niemann, H. B., et al. 1998, J. Geophys. Res., 103, 22831
Partridge, H., & Schwenke, D. 1997, J. Chem. Phys., 106, 4618
Saumon, D., et al. 2007, ApJ, 656, 1136
Schwenke, D. 1998, Faraday Discuss., 109, 321
Sharp, C. M., & Burrows, A. 2007, ApJS, 168, 140
Strong, K., Taylor, F. W., Calcutt, S. B., Remedios, J. J., & Ballard, J. 1993, J. Quant. Spectrosc. Radiat. Transfer, 50, 363
Visscher, C., Lodders, K., & Fegley, B. J. 2006, ApJ, 648, 1181
Wenger, Ch., & Champion, J.-P. 1998, J. Quant. Spectrosc. Radiat. Transfer, 59, 471
Zheng, C., & Borysow, A. 1995, ApJ, 441, 960